

# Platelet-targeted dual pathway antithrombotic inhibits thrombosis with preserved hemostasis

Donny Hanjaya-Putra,<sup>1,2</sup> Carolyn Haller,<sup>1,2</sup> Xiaowei Wang,<sup>3</sup> Erbin Dai,<sup>1,2</sup> Bock Lim,<sup>3</sup> Liying Liu,<sup>1</sup> Patrick Jaminet,<sup>4</sup> Joy Yao,<sup>3</sup> Amy Searle,<sup>3</sup> Thomas Bonnard,<sup>3</sup> Christoph E. Hagemeyer,<sup>3</sup> Karlheinz Peter,<sup>3</sup> and Elliot L. Chaikof<sup>1,2,5</sup>

<sup>1</sup>Department of Surgery, Beth Israel Deaconess Medical Center (BIDMC), Harvard Medical School, Boston, Massachusetts, USA. <sup>2</sup>Wyss Institute for Biologically Inspired Engineering, Harvard University, Boston, Massachusetts, USA.

<sup>3</sup>Baker Heart and Diabetes Research Institute, Melbourne, VIC 8008, Australia. <sup>4</sup>University Hospital, Freiburg, Germany.

<sup>5</sup>Harvard-MIT Division of Health Sciences and Technology, Cambridge, Massachusetts, USA.

Despite advances in antithrombotic therapy, the risk of recurrent coronary/cerebrovascular ischemia or venous thromboembolism remains high. Dual pathway antithrombotic blockade, using both antiplatelet and anticoagulant therapy, offers the promise of improved thrombotic protection; however, widespread adoption remains tempered by substantial risk of major bleeding. Here, we report a dual pathway therapeutic capable of site-specific targeting to activated platelets and therapeutic enrichment at the site of thrombus growth to allow reduced dosing without compromised antithrombotic efficacy. We engineered a recombinant fusion protein, SCE5-TAP, which consists of a single-chain antibody (SCE5) that targets and blocks the activated GPIIb/IIIa complex, and tick anticoagulant peptide (TAP), a potent direct inhibitor of activated factor X (FXa). SCE5-TAP demonstrated selective platelet targeting and inhibition of thrombosis in murine models of both carotid artery and inferior vena cava thrombosis, without a significant impact on hemostasis. Selective targeting to activated platelets provides an attractive strategy to achieve high antithrombotic efficacy with reduced risk of bleeding complications.

## Introduction

The risk of recurrent coronary/cerebrovascular ischemia or venous thromboembolism (VTE) remains high, but strategies that utilize single or combined antiplatelet and anticoagulant therapies carry a substantial risk of major bleeding with incomplete protection of thrombotic risk. The most common reason for combined antiplatelet and anticoagulant therapy is the coexistence of an indication for either drug. For example, 10% of patients undergoing percutaneous coronary intervention (PCI), with a requirement for dual antiplatelet therapy (DAPT) (1, 2), also have an indication for oral anticoagulation because of atrial fibrillation. Likewise, the development of an acute coronary syndrome or the need for primary prevention of coronary artery disease, where antiplatelet therapy would be required, is common among patients with atrial fibrillation, a prosthetic heart valve, or a recent VTE (3–5). In the US, approximately 800,000 patients with atrial fibrillation are receiving a concomitant oral anticoagulant and antiplatelet therapy. Any combination of oral anticoagulants and antiplatelet therapy substantially increases the risk of bleeding and intracranial hemorrhage compared with either alone (6–11). The newer antiplatelet drugs are more effective than clopidogrel but are not safer and may even exacerbate bleeding risk (12), and no significant difference in major bleeding has been observed between the new oral anticoagulants and warfarin (7, 13–15). Moreover, despite the frequent use of combined antiplatelet therapy and anticoagulation in patients with atrial fibrillation, the rates of thrombotic events remain high in the post-PCI setting (16). These patients are at very high risk for bleeding events but need more potent therapies to address their high thrombotic event rate (17).

The objective of this study was to develop a dual pathway therapeutic capable of concentrating antiplatelet and anticoagulant activity at the site of a primary platelet deposition. Conventional doctrine describes early platelet adhesion and aggregation events mediated by collagen and von Willebrand factor (VWF) engagement of platelet glycoprotein VI (GPVI) or GPIb receptors, which leads to the formation of

**Authorship note:** DHP, CH, and XW contributed equally to this work. KP and ELC contributed equally as co-senior authors.

**Conflict of interest:** The authors have declared that no conflict of interest exists.

**Submitted:** December 18, 2017

**Accepted:** June 28, 2018

**Published:** August 9, 2018

**Reference information:**

*JCI Insight.* 2018;3(15):e99329.

<https://doi.org/10.1172/jci.insight.99329>

insight.99329.

an initial platelet plug followed by platelet activation with the presentation of a procoagulant surface that supports the initiation and propagation of the coagulation cascade. Recent reports have contributed further insight toward the earliest events driving platelet adhesion to the vascular wall. Significantly, rheological-dependent platelet aggregation has been described, which occurs without detectable activation markers such as shape change, calcium signaling, and  $\alpha$ -granule secretion (18–20). This provides strong motivation to develop a strategy targeted to activated platelets that would allow reduced dosing regimens and provide limited risk toward impeding either matrix-driven adhesion or shear-induced mechanosensitive adhesion that is critical to hemostasis. Toward this aim, we have engineered a recombinant fusion protein, SCE5-TAP, as a dual pathway inhibitor, which consists of a single-chain antibody (SCE5) that targets and blocks the activated GPIIb/IIIa complex and tick anticoagulant peptide (TAP), a potent direct inhibitor of FXa.

The GPIIb/IIIa complex is the most abundant protein expressed on the platelet surface. Upon platelet activation, the conformational change of GPIIb/IIIa from a low- to high-affinity fibrinogen binding state exposes new epitopes that has facilitated the generation of SCE5, which specifically binds to activated platelets but not to nonactivated platelets in circulation (21). Selective targeting to activated platelets ensures enrichment at a growing thrombus. Moreover, SCE5 targeting and blockade of the activated GPIIb/IIIa complex begins only after the initial platelet seal has been established, thereby maintaining normal hemostasis (22). We have combined conformation-specific GPIIb/IIIa blockade with TAP, a potent direct inhibitor of FXa. FXa is a key driver of thrombin activation, and anti-FXa strategies have received intense investigation as a means to prevent and treat thrombotic disease. “Triple therapy,” composed of a dual pathway approach with antiplatelet therapy (P2Y<sub>12</sub> inhibitor plus aspirin) and oral anticoagulation, has led to a reduction in cardiovascular mortality (23–25). However, the increased risk of major bleeding has prevented widespread adoption of this approach (6, 23, 24, 26). With selective and site-specific targeting to activated platelets after platelet plug formation, we present a potentially novel strategy to broaden the therapeutic potential of dual pathway inhibition with improved safety.

## Results

*SCE5-TAP demonstrates antiplatelet and anticoagulant activity.* The objective of this study was to develop a dual pathway therapeutic capable of concentrating antiplatelet and anticoagulant activity at the site of clot formation. Recent reports have drawn a mechanistic distinction between primary platelet adhesion, which occurs without platelet activation, as reflected in the absence of activation markers, such as shape change, calcium signaling, or  $\alpha$ -granule secretion and secondary platelet adhesion and aggregation, driven by traditional soluble mediators of activation (18–20, 27). Primary platelet adhesion mediates the formation of a hemostatic seal, whereas secondary platelet adhesion and aggregation resulting from unrestrained platelet activation may lead, ultimately, to occlusive thrombosis. GPIIb/IIIa in its nonactivated state can mediate binding to immobilized fibrinogen and, thus, supports primary platelet adhesion without the necessity of GPIIb/IIIa to be in its activated conformation. This provides a potentially novel therapeutic opportunity to develop a targeting strategy that is specific to the activated GPIIb/IIIa receptor, concentrating platelet and coagulation pathway inhibitors at the site of activated platelets. This enables drug administration at reduced systemic dosing regimens and avoids interference with primary platelet adhesion that is critical to the formation of an initial platelet seal and, as a consequence, for hemostasis. Toward this aim, we engineered a recombinant fusion protein, SCE5-TAP, which consists of a single-chain antibody (SCE5) that targets the activated GPIIb/IIIa complex, and TAP, a potent direct inhibitor of FXa. SCE5 was isolated using phage display in concert with depletion and selection protocols to identify a single chain antibody that selectively binds activated platelets but displays no binding affinity toward nonactivated platelets (21). TAP DNA was synthesized (28) and cloned in frame to the C-terminus of SCE5. In addition, we generated a control construct, MUT-TAP, which consists of a mutated single-chain variable fragment (scFv; MUT), generated by alanine substitution mutagenesis of heavy-chain CDR3, which displays no platelet binding activity (21), fused with active TAP. Recombinant expression was performed in *Drosophila* pMT/BiP/V5-His, and constructs were purified using metal affinity and size exclusion chromatography (Supplemental Figure 1).

Selective binding to activated platelets was confirmed using flow cytometry. SCE5, SCE5-TAP, or MUT-TAP were incubated with resting or 20  $\mu$ M ADP-activated human or mouse platelets, and binding was assessed using anti-His-mAb-AF488. We observed activation-specific binding of SCE5 to both human and mouse platelets, with no binding to resting platelets (Figure 1, A and D). Fusion construct SCE5-TAP

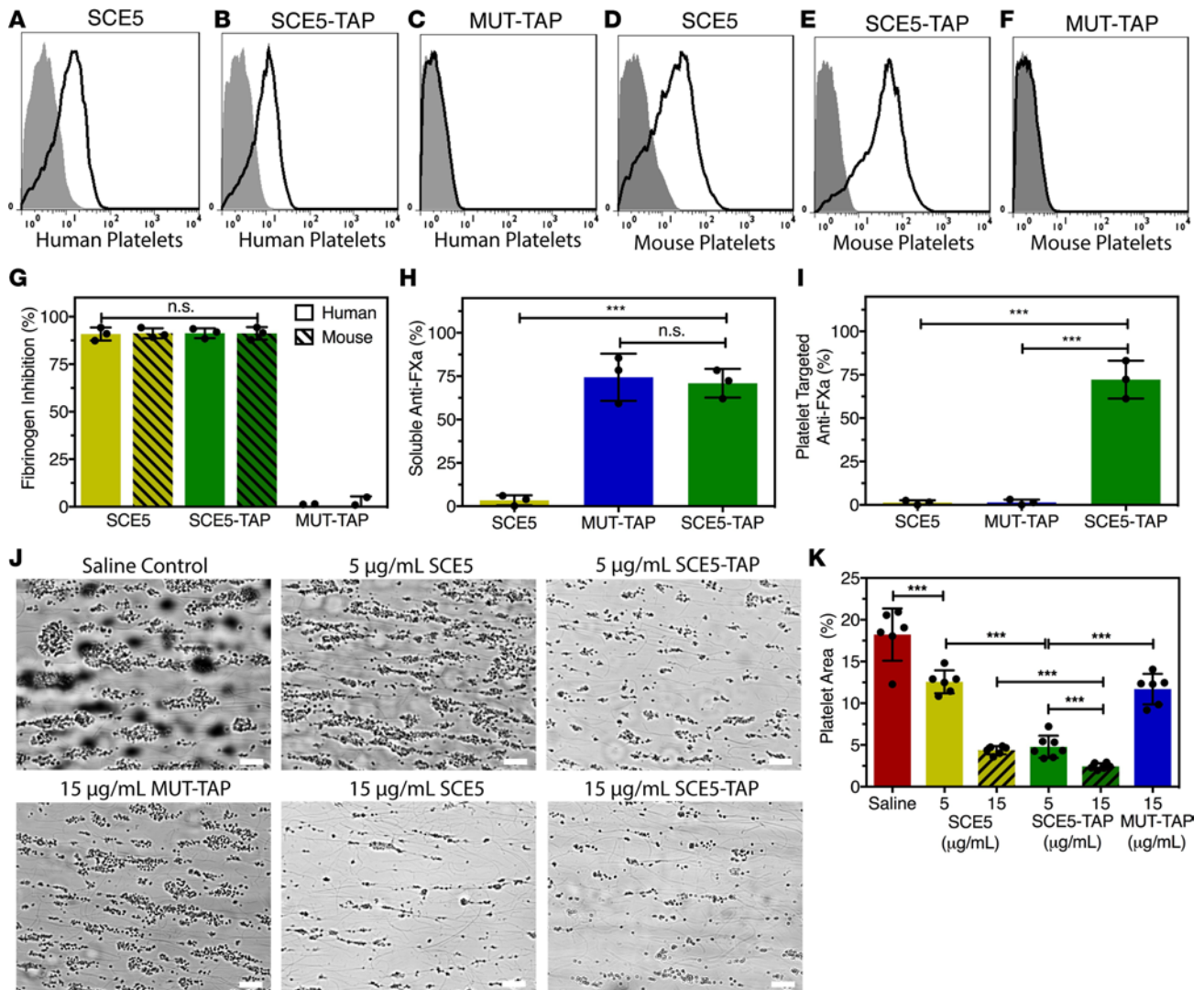


**Figure 1. Characterization of SCE5-TAP antiplatelet and anticoagulant activity.** Selective targeting to ADP-activated human (A–C) or mouse (D–F) platelets was assessed by flow cytometry. Construct binding to activated platelets (white histogram) or nonactivated platelets (gray histogram) was detected by AF488 anti-His antibody. SCE5 and SCE5-TAP target human (A and B) or mouse (D and E) activated platelets, while MUT-TAP displays no binding (C and F). Representative histograms are shown from 4 experiments. (G) GPIIb/IIIa blocking activity was examined through flow cytometry analysis of fibrinogen binding to human and mouse ADP-activated platelets. Fibrinogen binding was quantified as mean fluorescent intensity, and % inhibition was calculated relative to vehicle control;  $n = 4$ . (H and I) Anti-FXa activity was monitored using chromogenic FXa substrate in solution (H) and after targeting constructs to fibrinogen-adherent activated platelets (I). Percent inhibition of FXa was calculated relative to vehicle control with measurements performed in triplicate;  $n = 4$  experiments. (J and K) Flow chamber adhesion assay was performed with perfusion ( $500 \text{ s}^{-1}$ ) of whole blood over collagen-coated glass capillaries (J). Phase contrast images of microthrombi formed in presence of SCE5 (5 and 15  $\mu\text{g}/\text{mL}$ ), SCE5-TAP (5 and 15  $\mu\text{g}/\text{mL}$ ), MUT-TAP (15  $\mu\text{g}/\text{mL}$ ), or saline vehicle. Scale bars: 20  $\mu\text{m}$ . (K) Microthrombi were captured at 20 $\times$  and area quantified with ImageJ;  $n = 4$  per group. Data represent mean  $\pm$  SD, \*\*\* $P \leq 0.001$  (ANOVA and Bonferroni's multiple comparison test).

also displayed activation-specific binding (Figure 1, B and E), while platelet binding was not observed with the MUT-TAP control construct (Figure 1, C and F). These results confirm that C-terminal TAP fusion does not impede scFv targeting to activated GPIIb/IIIa receptors and, thus, to activated platelets. SCE5-TAP selective binding to activated platelets was further confirmed with additional platelet agonists, including collagen related peptide (CRP) and thrombin receptor-activating peptide (TRAP) (Supplemental Figure 2). Because SCE5 also serves as a conformation-specific inhibitor of GPIIb/IIIa, we examined the ability of fusion constructs to inhibit fibrinogen binding to activated platelets. Human or mouse PRP ( $\pm 20 \mu\text{M}$  ADP) was incubated with SCE5, SCE5-TAP, MUT-TAP, or vehicle control, and fibrinogen binding was detected using flow cytometry with FITC-labeled anti-fibrinogen antibody. We defined maximum fibrinogen binding with respect to the fluorescent shift detected in 20  $\mu\text{M}$  ADP-activated vehicle control,

with results plotted as percent inhibition (Supplemental Figure 3). We observed significant inhibition of fibrinogen binding with both SCE5 and SCE5-TAP, confirming activation-specific blockade of GPIIb/IIIa (Figure 1G). There was no significant difference between SCE5 and SCE5-TAP, indicating no impairment of the SCE5 GPIIb/IIIa blocking function by C-terminal TAP fusion. No inhibition was observed with MUT-TAP. Inhibition of fibrinogen binding by SCE5-TAP was also characterized with platelet agonists CRP and TRAP (Supplemental Figure 4). Light transmission aggregometry was also performed to examine the ability of fusion proteins to inhibit platelet aggregation. At a concentration of 15  $\mu\text{g/ml}$ , SCE5 and SCE5-TAP demonstrated strong inhibition of ADP-induced platelet aggregation, while MUT-TAP showed no inhibitory effect (Supplemental Figure 5).

We characterized anti-FXa activity to confirm functional integrity of the TAP fusion. The soluble activity of constructs was assessed by incubating SCE5-TAP with purified FXa and a chromogenic, Xa-specific substrate. Results are reported as percent inhibition of FXa relative to vehicle control. SCE5-TAP and MUT-TAP inhibited FXa equally, while inhibition was not observed with scFv SCE5 (Figure 1H). Additionally, we confirmed retention of anti-FXa activity when SCE5-TAP was bound to a fibrinogen-adherent platelet-covered surface (Figure 1I). Finally, a flow chamber adhesion assay was employed to examine the effect of dual pathway inhibition in whole blood. To mimic initial platelet adhesion and consequent platelet aggregation, blood was perfused over collagen fibers in the presence of SCE5, SCE5-TAP, MUT-TAP, or saline control, and platelet adhesion/aggregation was assessed using bright field microscopy. As compared with saline control, SCE5 at 5  $\mu\text{g/ml}$  produced a slight reduction of platelet aggregates, while an equivalent dose of SCE5-TAP nearly fully eliminated platelet aggregate formation (Figure 1, J and K). Only when blood was perfused with SCE5 at a 3-fold-higher concentration (15  $\mu\text{g/ml}$ ) was a nearly full reduction of platelet microthrombi observed. The enhanced efficacy of the fusion construct highlights the advantage of TAP fusion to SCE5 with dual pathway blockade. Significantly, we continued to observe platelet adhesion to collagen fibers in the presence of both SCE5 and SCE5-TAP, suggesting that primary platelet attachment to collagen was not impeded.

*SCE5-TAP targets arterial thrombus and inhibits occlusion in mice.* The capacity of SCE5-TAP to target and limit arterial thrombus formation was investigated using intravital microscopy (IVM) of localized laser-induced injury to murine cremaster arterioles (Figure 2, A–C). To characterize targeting, SCE5-TAP and MUT-TAP were incubated with anti-His AF488 to label construct His tags. Mice were infused with platelet-specific Dylight 649-labeled anti-CD42b and AF488-SCE5-TAP, AF488-MUT-TAP, or anti-His AF488 control and subject to laser injury. Platelet thrombi targeting, as indicated by fluorescent colocalization, was only observed with AF488-SCE5-TAP infusion (Supplemental Figure 6). We next investigated the capacity of SCE5-TAP to limit arterial thrombus formation. Laser injury was performed with quantitative analysis of Dylight 649-labeled platelets. I.v. infusion of MUT-TAP (0.03  $\mu\text{g/g}$ ) resulted in little change in platelet accumulation as compared with the saline vehicle. However, infusion of SCE5-TAP (0.03  $\mu\text{g/g}$ ) resulted in significant reduction in platelet deposition at the site of vessel wall injury (Figure 2, A–C).

To examine efficacy in a larger diameter artery, constructs were studied in a ferric chloride-induced ( $\text{FeCl}_3$ -induced) arterial thrombosis model of the left common carotid artery (29). Thrombus targeting was confirmed using IVIS in vivo imaging with IR800-labeled SCE5-TAP (Figure 2D and Supplemental Figure 7). Vessel flow was monitored for a maximum of 30 minutes, and both enoxaparin (low molecular weight heparin; LMWH) and eptifibatid (Ept) were included as clinically relevant standards that block FXa or platelet GPIIb/IIIa receptors, respectively. Carotid artery occlusion was noted within  $\sim 10$  minutes ( $10.2 \pm 1.6$  min) for those animals treated with saline alone, while administration of SCE5-TAP at a dose that proved efficacious in the IVM laser injury model (0.03  $\mu\text{g/g}$ ) significantly delayed arterial occlusion ( $24.8 \pm 3.3$  min) (Figure 2E). In contrast, administration of MUT-TAP (0.03  $\mu\text{g/g}$ ) did not affect occlusion time. At a 10-fold higher dosing regimen (0.3  $\mu\text{g/g}$ ) of SCE5-TAP, we continued to observe a significant prolongation in occlusion time, while the effect of MUT-TAP (0.3  $\mu\text{g/g}$ ) and SCE5 (0.3  $\mu\text{g/g}$ ) were similar to saline control (Figure 2E). Tail transection bleeding time was evaluated to examine whether hemostasis is maintained or impaired by the administered agents. At a therapeutic dose of 0.03  $\mu\text{g/g}$ , SCE5-TAP did not increase either bleeding time or bleeding volume when compared with saline vehicle (Figure 2, F and G). Reference agents, enoxaparin and Ept, administered at clinically relevant dosing levels, demonstrated both significant thrombus inhibition and marked impairment in hemostasis. A smaller but statistically significant increase in bleeding time and bleeding volume were observed at the highest dose (0.3  $\mu\text{g/g}$ ) of SCE5-TAP and MUT-TAP, while increased bleeding was not observed with administration of SCE5 (Figure 2,

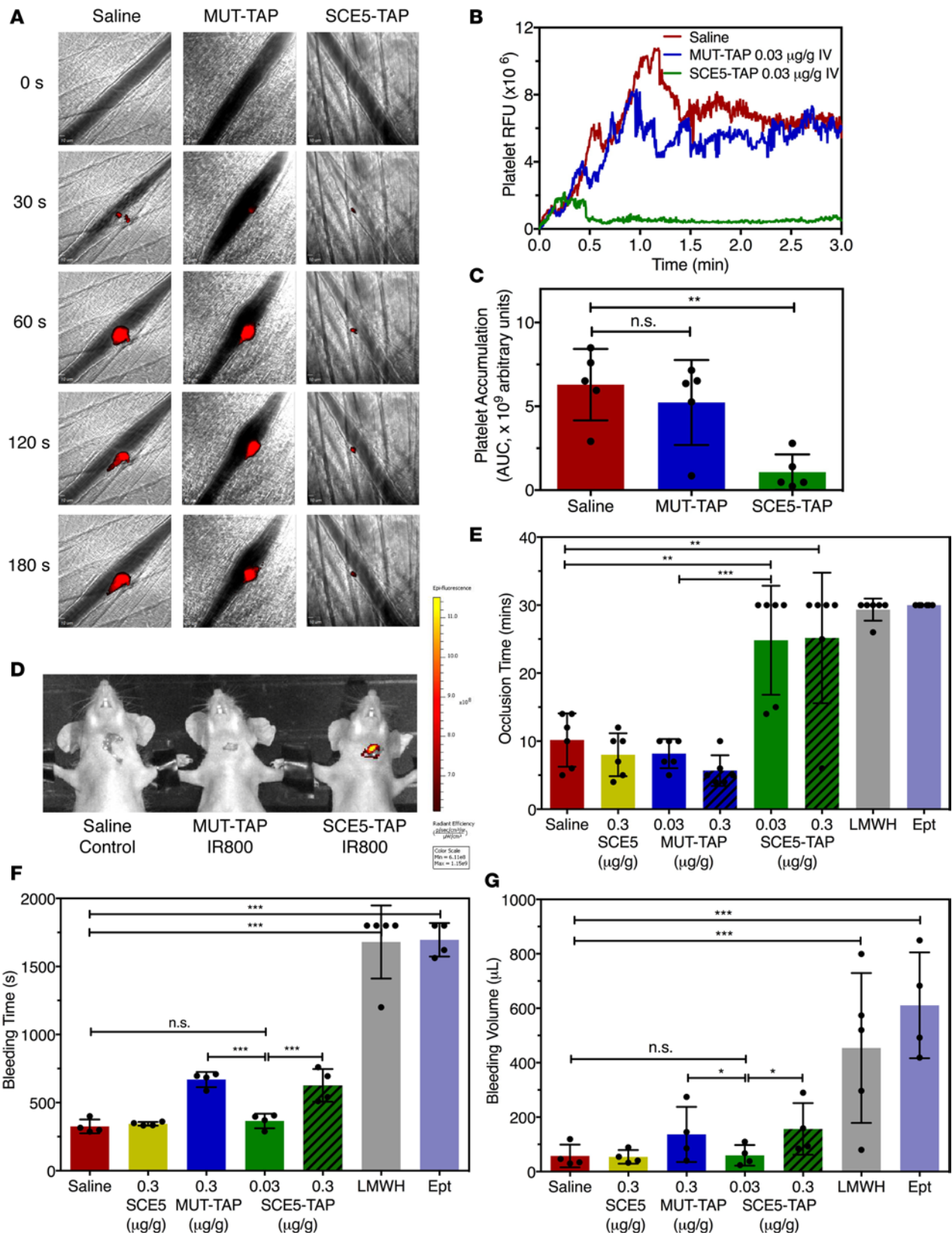


**Figure 2. SCE5-TAP targets arterial thrombus and inhibits occlusion in mice.** Platelet-specific anti-CD42b-Dylight 649 was infused and thrombus formation induced by laser injury and was characterized over time. (A) Representative images of the fluorescence signal associated with platelet thrombus after laser injury of cremaster arterioles. Saline, MUT-TAP (0.03 µg/g), or SCE5-TAP (0.03 µg/g) were administered (i.v.) up to 30 minutes prior to laser injury. (B) Median integrated platelet fluorescence with administration of saline (red), MUT-TAP (blue), or SCE5-TAP (green). (C) Platelet accumulation was quantified as the AUC as calculated for platelet relative fluorescence units (RFU). Units are arbitrary and data represent mean ± SD,

$n = 20$ – $34$  vessels in 4–5 mice/group. (D) Carotid artery thrombosis was induced with ferric chloride, and construct targeting was confirmed using IVIS scan with IR800-labeled MUT-TAP or SCE5-TAP. (E) Ferric chloride-induced carotid artery thrombus development was monitored with a nano-flow probe. A significant increase in occlusion time was observed with SCE5-TAP (0.03 and 0.3  $\mu\text{g/g}$ ) and with reference compounds LMWH (enoxaparin, 10  $\mu\text{g/g}$ ) and Ept (eptifibatide, 10  $\mu\text{g/g}$ ). Tail transection performed 1 minute after i.v. administration revealed a significant prolongation of (F) bleeding time and (G) bleeding volume for reference agents, LMWH (enoxaparin, 10  $\mu\text{g/g}$ ), and Ept (eptifibatide, 10  $\mu\text{g/g}$ ), but not for SCE5-TAP (0.03  $\mu\text{g/g}$ ). Data represent mean  $\pm$  SD,  $n = 4$  per group, \* $P \leq 0.05$ , \*\* $P \leq 0.01$ , and \*\*\* $P \leq 0.001$  (ANOVA and Bonferroni's multiple comparison test).

F and G). Collectively, these data demonstrate the potential to target a dual pathway inhibitor to activated platelets using a lower yet efficacious dosing regimen, which limits the risk of increased bleeding associated with conventional anticoagulants.

*SCE5 inhibits mouse models of venous thrombosis.* Prior to initiating enrollment of SCE5-TAP in a model of venous thrombosis, we explored the influence of the administration route on circulating drug half-life. SCE5-TAP was administered via s.c. or i.v. routes, and circulating anti-FXa in plasma was monitored over time. Results were compared with an in vitro standard curve of anti-FXa activity as a function of SCE5-TAP concentration. S.c. delivery significantly extended the circulating half-life of SCE5-TAP from  $2.75 \pm 0.15$  hours (i.v.) to  $10.13 \pm 1.07$  hours (s.c.) (Figure 3A). IVM of localized laser-induced injury to cremaster venules was used to investigate targeting and the antithrombotic profile. Construct targeting to activated platelets at sites of venule wall injury was confirmed with infusion of Dylight 649-labeled anti-CD42b and AF488-SCE5-TAP, AF488-MUT-TAP, or anti-His AF488 control. Time-lapse analysis demonstrates delayed binding of AF488-SCE5-TAP to an established Dylight 649 platelet surface, suggesting that SCE5 does not inhibit the initial sealing layer of platelets (Supplemental Figure 8). Moreover, fluorescence colocalization of platelet Dylight 649 and construct AF488 signal was only observed with AF488-SCE5-TAP administration (Figure 3B). Noting peak circulating anti-FXa activity 4 hours after s.c. administration of SCE5-TAP (Figure 3A), inhibition of venule thrombus formation was assessed at this time point. Studies were initially performed to verify a therapeutic effect of SCE5-TAP and to determine the lowest effective i.v. (0.05  $\mu\text{g/g}$ ) or s.c. (0.1  $\mu\text{g/g}$ ) dose when laser injury was performed immediately or 4 hours after drug administration, respectively (Supplemental Figure 9). Significant reduction in venous platelet accumulation was achieved with SCE5-TAP (0.1  $\mu\text{g/g}$  s.c.), while MUT-TAP (0.1  $\mu\text{g/g}$  s.c.) and equimolar SCE5 (0.06  $\mu\text{g/g}$  s.c.) displayed no inhibitory effect (Figure 3, C and D). LMWH (4  $\mu\text{g/g}$  s.c.) was dosed according to recommended clinical guidelines for peak anti-FXa activity (0.4–0.6 IU/ml), as required for prevention of VTE (Figure 3E) (30). Notably, the antithrombotic activity of SCE5-TAP was equivalent to that observed for LMWH, but at a significantly lower peak level of circulating anti-FXa (Figure 3, D and E). We next explored a SCE5-TAP dosing strategy that would sustain antithrombotic activity up to 24 hours after administration. Significant reduction in venous platelet accumulation was achieved at a 5-fold increased concentration of SCE5-TAP (0.5  $\mu\text{g/g}$  s.c.), while MUT-TAP (0.5  $\mu\text{g/g}$  s.c.) and equimolar SCE5 (0.3  $\mu\text{g/g}$  s.c.) displayed no inhibitory activity (Figure 3, F and G). Peak circulating anti-FXa activity remained low relative to LMWH (Figure 3H), suggesting that therapeutic SCE5-TAP would be associated with reduced bleeding risk.

We employed this prophylactic administration strategy to evaluate the capacity of SCE5-TAP to limit murine deep venous thrombosis using an electrolytic inferior vena cava model (EIM). Murine venous thrombosis models are well reviewed (31, 32). We specifically selected EIM to achieve reproducible and nonocclusive inferior vena cava (IVC) thrombus, formed in the presence of blood flow (33). We administered SCE5-TAP (0.5  $\mu\text{g/g}$  s.c.) or the clinically relevant anti-FXa therapeutics, LMWH (4  $\mu\text{g/g}$  s.c.) or rivaroxaban (1  $\mu\text{g/g}$  per os), 4 hours prior to electrolytic injury and 24 hours after injury. Controls included saline vehicle, uninjured IVC, and surgical sham with needle insertion into the IVC but without induction of current (sham no current) (data not shown). A uniform length of IVC was harvested 48 hours after injury and immediately weighed to measure vessel wall and thrombus weight (TW). SCE5-TAP displayed 43.24%  $\pm$  4.09% thrombus inhibition as compared with saline vehicle, which was comparable with the effect observed for LMWH (47.31%  $\pm$  3.58%) and rivaroxaban (42.09%  $\pm$  2.50%) (Figure 4, A and B). Harvested IVC cross sections were stained, and the thrombus area was measured. Treatment groups displayed an approximately 45% reduction in thrombus area without a significant difference between SCE5-TAP, LMWH, and rivaroxaban (Figure 4, C and D). Bleeding risk was assessed by measuring peak circulating anti-FXa activity (Supplemental Figure 10) and by determining tail transection bleeding time and blood loss, 4 hours after drug administration. At therapeutic dosing, SCE5-TAP displayed minimal circulating anti-FXa activity and no increase in bleeding time or blood loss volume as compared with saline vehicle.

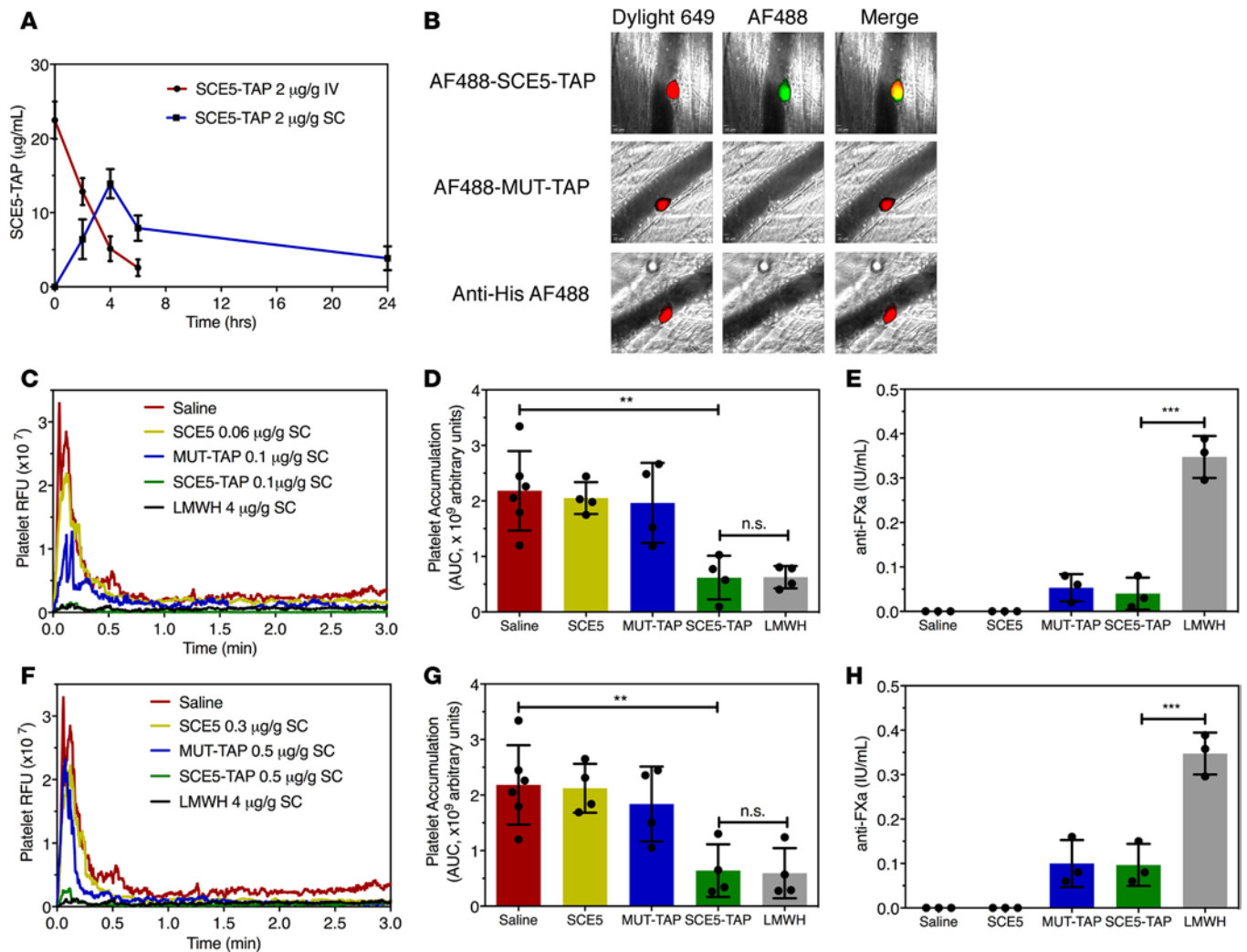


**Figure 3. SCE5-TAP targets venous platelets and inhibits venous thrombosis in vivo.** (A) Systemic concentration of SCE5-TAP over time with i.v. or s.c. delivery. Concentrations were characterized based on circulating anti-FXa activity and compared with a standard curve. (B–H) SCE5-TAP targets and reduces venous thrombosis after laser injury of cremaster venules. (B) Platelet-specific Dylight 649-labeled anti-CD42b was infused with AF488-labeled SCE5-TAP (top row), AF488-labeled MUT-TAP (middle row), or AF488 control (bottom row) prior to laser injury of cremaster venules. Representative images illustrate that SCE5-TAP targets platelets within the venous thrombus. Colocalization of MUT-TAP or AF488 control was not observed. (C–D) SCE5-TAP efficiently reduces venous thrombus at a dose administration of 0.1 µg/g s.c. (solid green, thrombus inhibition characterized 4 hours after s.c. administration). Results are compared with equivalent doses of MUT-TAP (s.c.) or LMWH (enoxaparin, 4 µg/g s.c.), 4 hours after s.c. administration. Results are plotted as median integrated platelet fluorescence (C) or platelet accumulation quantified as AUC (D);  $n = 20\text{--}34$  vessels in 4–5 mice/group. (E) Circulating anti-FXa activity was measured for each agent (data collected 4 hours after s.c. administration). Data represent mean  $\pm$  SD,  $n = 4$  per group. (F and G) SCE5-TAP reduces venous thrombus formation 24 hours after s.c. administration. The dose of SCE5-TAP was increased to 0.5 µg/g s.c. (dark green), and laser injury of cremaster venules was performed 24 hours later. Results are compared with equivalent doses of MUT-TAP (blue, 0.5 µg/g s.c.), equimolar SCE5 (yellow, 0.3 µg/g s.c.), or LMWH (black, 4 µg/g s.c.). Results are plotted as median integrated platelet fluorescence (F) or platelet accumulation quantified as AUC (G);  $n = 20\text{--}34$  vessels in 4–5 mice/group. (H) Circulating anti-FXa activity was measured for each s.c. dose 4 hours after administration. Data represent mean  $\pm$  SD,  $n = 4$  per group. All  $P$  values were determined by ANOVA and Bonferroni's multiple comparison test,  $**P \leq 0.01$ , and  $***P \leq 0.001$ .

Therapeutic dosing of LMWH and rivaroxaban, consistent with clinical guidelines for prevention of VTE, was associated with increased bleeding (Figure 4, E–G). Of note, a 10-fold increase in MUT-TAP (5 µg/g s.c.) was necessary to achieve a therapeutic effect comparable with SCE5-TAP (0.5 µg/g s.c.) but with significant impairment in hemostasis (Supplemental Figure 11). Collectively, these results highlight the advantage of selective targeting to reduce the dose and limit bleeding-risk associated with conventional dual pathway blockade through combined anticoagulation and antiplatelet regimens.

To analyze the corresponding inflammatory response 48 hours after EIM, a uniform length of IVC and thrombus was harvested and digested to a single cell suspension for flow cytometry analysis of

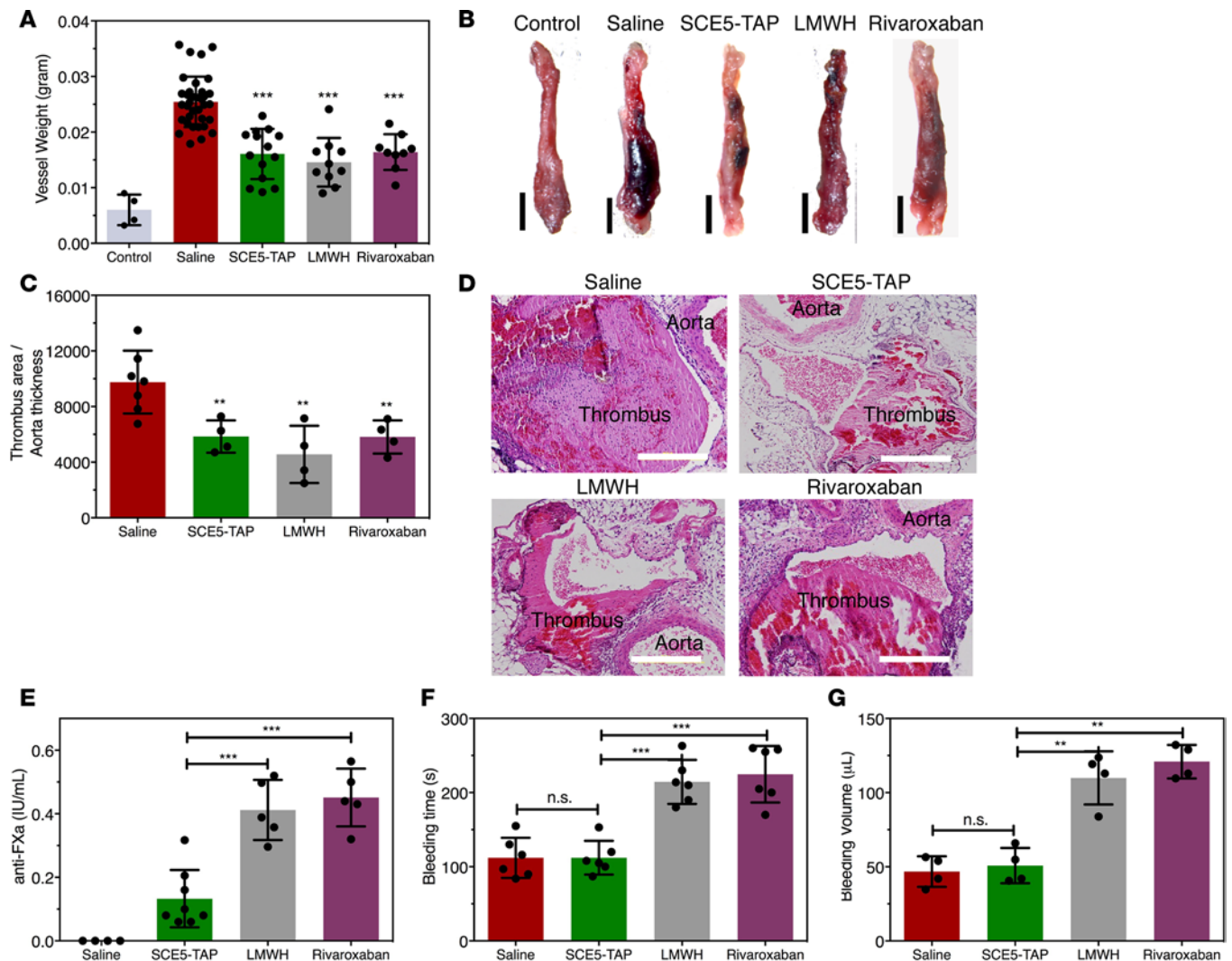


**Figure 4. SCE5-TAP inhibits deep venous thrombosis without increased bleeding risk.** An electrolytic IVC model (EIM) was used to generate a nonocclusive venous thrombus in the IVC. SCE5-TAP (0.5  $\mu\text{g/g}$  s.c.), LMWH (4  $\mu\text{g/g}$  s.c.), or Rivaroxaban (1  $\mu\text{g/g}$  per os) were administered 4 hours prior to electrolytic injury and 24 hours after injury. The IVC was harvested at 48 hours for thrombus characterization. (**A** and **B**) A uniform length of IVC was harvested and immediately weighed to determine vessel wall and thrombus weight. Control enrollment included uninjured IVC without thrombus induction;  $n = 10$ –35 mice/group. Data represent mean  $\pm$  SD,  $***P \leq 0.001$  vs. saline control. (**C** and **D**) Thrombus area was characterized from H&E-stained sections. Thrombus area is reported as area ( $\text{mm}^2$ )/aortic wall thickness (mm);  $n = 5$  mice/group, 3 sections/mouse. Data represent mean  $\pm$  SD,  $**P \leq 0.01$  vs. saline control. Scale bars: 500  $\mu\text{m}$ . (**E**–**G**) Systemic bleeding risk was characterized 4 hours after administration of test compound by measuring circulating anti-FXa activity (**E**), tail transection bleeding time (**F**), and tail transection blood loss (**G**);  $n = 5$ –10 mice/group. Data represent mean  $\pm$  SD,  $**P \leq 0.01$  and  $***P \leq 0.001$ . All  $P$  values were determined by ANOVA and Bonferroni's multiple comparison test.

total leukocytes ( $\text{CD45}^+$ ), platelets ( $\text{CD41}^+$ ), neutrophils ( $\text{CD11b}^+/\text{Ly6G}^+$ ), and monocytes ( $\text{CD11b}^+/\text{Ly6G}^-$ ). A representative gating strategy is provided in Supplemental Figure 12. We observed significant reductions in total leukocytes, neutrophils, and monocytes with SCE5-TAP, LMWH, and rivaroxaban relative to saline vehicle (Figure 5, A, C, and D). Results were reported as absolute cell number relative to vessel wall weight to reflect the concentration of leukocytes per thrombus. These results suggest that reduced leukocyte content in treatment groups is not simply a function of thrombus trapping, but rather may be a downstream benefit of anti-FXa treatment and reduced production of proinflammatory mediators, such as thrombin. The reduction of neutrophils (Figure 5C) is consistent with their dominant and early role in vessel wall inflammation after thrombus formation (33). We also observed a significant reduction in platelet accumulation across all treatment groups (Figure 5B). Standard IHC was performed on paraffin-embedded IVC sections to characterize inflammatory cell localization. Leukocyte and platelet staining were localized to the luminal thrombus in all groups (Figure 5, E–G).

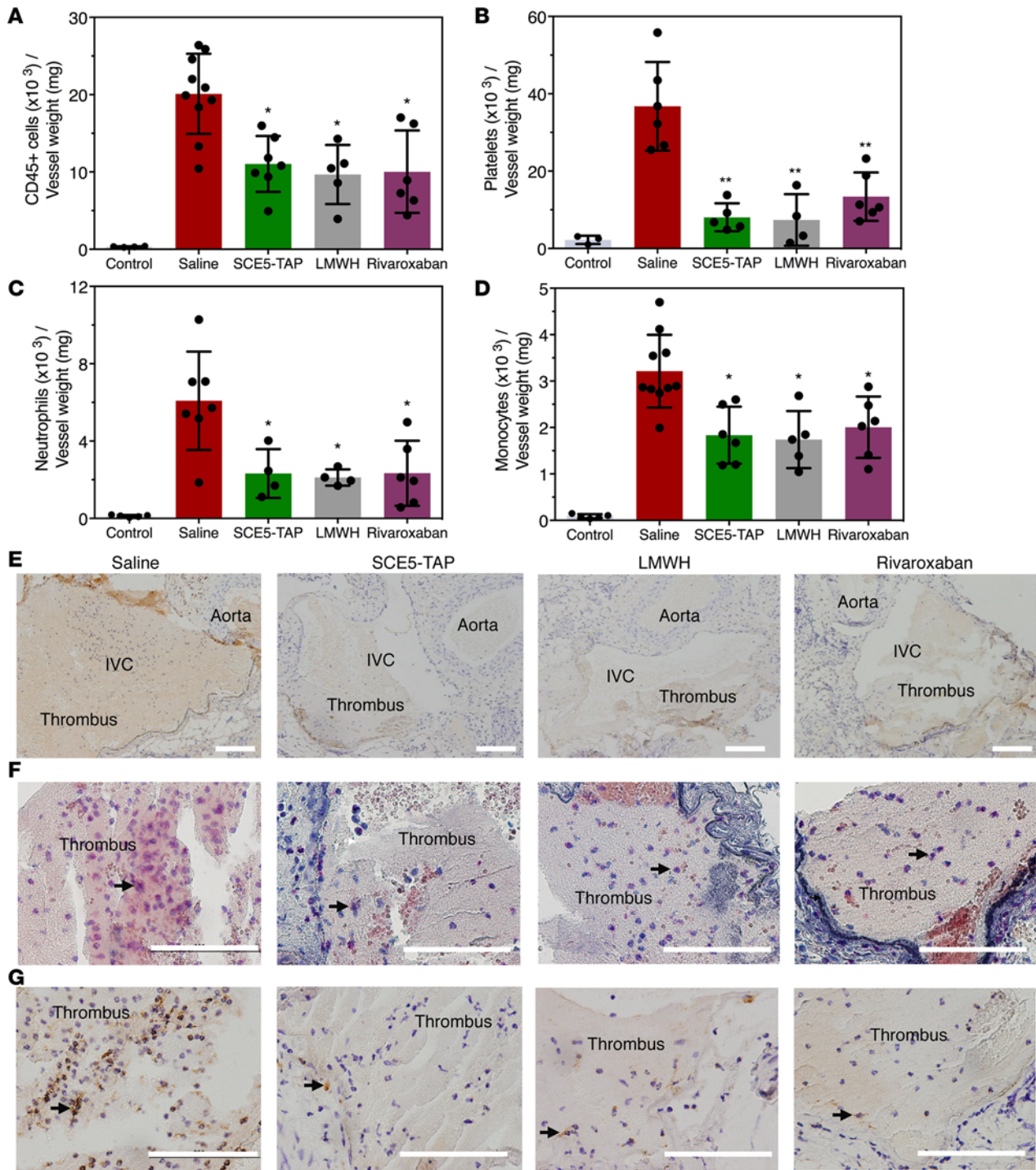


**Figure 5. DVT-associated inflammatory response.** (A–D) A uniform length of IVC wall and associated thrombus were harvested 48 hours after electrolytic injury and digested to a single cell suspension for flow cytometry analysis of total leukocytes (A) (CD45<sup>+</sup>), platelets (B) (CD41<sup>+</sup>), neutrophils (C) (CD11b<sup>+</sup>/Ly6G<sup>+</sup>), and monocytes (D) (CD11b<sup>+</sup>/Ly6G<sup>+</sup>). Results are reported as absolute cell number relative to vessel wall weight;  $n = 5-10$  mice/group. Data represent mean  $\pm$  SD, \* $P \leq 0.05$  and \*\* $P \leq 0.01$  vs. saline control (ANOVA and Bonferroni’s multiple comparison test). (E–G) IHC was performed on paraffin-embedded IVC sections to characterize inflammatory cell localization. (E) CD41<sup>+</sup> platelets, (F) neutrophil esterase<sup>+</sup>, and (G) CD68<sup>+</sup> monocytes. Scale bars: 100  $\mu$ m. Black arrows indicate positive staining.

*SCE5-TAP provides an improved therapeutic window for treatment of deep venous thrombosis.* To define a therapeutic index for SCE5-TAP, LMWH, and rivaroxaban, we investigated the dose-dependent inhibition of IVC thrombosis in relation to tail transection bleeding time. Agents were administered 4 hours prior to and 24 hours after injury, with TW assessed 48 hours after injury. Circulating anti-FXa activity confirmed peak

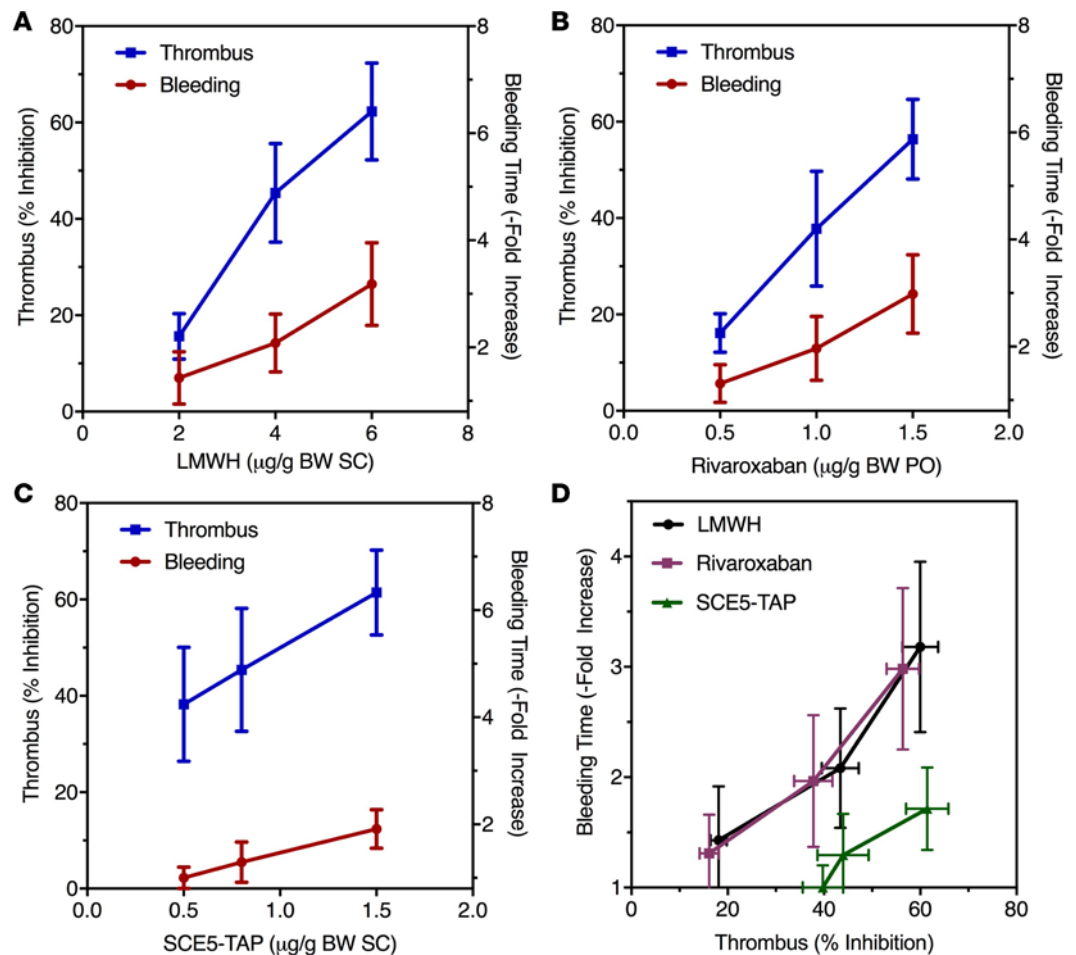


**Figure 6. Dose-dependent inhibition of IVC thrombosis versus tail transection bleeding time.** (A–C) Antithrombotic efficacy (% inhibition) is calculated based on percent reduction of thrombus weight in treatment groups vs. saline control 48 hours after electrolytic injury of the IVC. Bleeding time is reported as fold-increase in tail transection bleeding time over saline control, 4 hours after administration of the test agent. (A) LMWH (enoxaparin, 2–6 µg/g s.c.), (B) rivaroxaban (0.5–1.5 µg/g per os), (C) SCE5-TAP (0.5–1.5 µg/g s.c.), and (D) plot of thrombus reduction vs. corresponding bleeding time for LMWH, rivaroxaban, and SCE5-TAP. Data represent mean ± SD,  $n = 5$ –15 per treatment dose for thrombus inhibition studies and  $n = 4$ –6 per treatment dose for bleeding time studies.

anti-FXa activity 4 hours after administration (Supplemental Figure 10). Dose relationship studies were initiated to identify maximum achievable thrombus inhibition with the reference therapeutics, LMWH (s.c.) or rivaroxaban (per os). For both agents, a maximum inhibition of 60% was observed, with higher dosing regimens limited by increased bleeding risk. We achieved 60% thrombus inhibition at 1.5 µg/g SCE5-TAP (s.c.) with a corresponding 1.71 ± 0.17-fold increase in bleeding time (Figure 6C). Equivalent inhibition with LMWH (6 µg/g s.c.) or rivaroxaban (1.5 µg/g per os) resulted in a 3.16 ± 0.31-fold and 2.98 ± 0.33-fold increase in bleeding time, respectively (Figure 6, A and B). For antithrombotic agents, a smaller dose response slope of thrombus inhibition related to bleeding time is favorable because it offers reduced risk of excessive bleeding. SCE5-TAP administration demonstrated a dose response slope of 6.11, while the slopes for LMWH and rivaroxaban were 10.47 and 10.05, respectively. Despite dual pathway inhibition, statistical analysis confirmed a significantly lower dose response slope for SCE5-TAP as compared with LMWH ( $P = 0.0098$ ) or rivaroxaban ( $P = 0.001136$ ), with an efficacy-to-bleeding profile suggesting a greater safety margin for SCE5-TAP treatment of venous thrombosis (Figure 6D). Following the characterization of percent thrombus inhibition and bleeding time for SCE5-TAP doses ranging between 0.5 and 1.5 µg/g, we performed an equimolar dose escalation study of the single-chain antibody alone (SCE5) and nontargeted TAP (MUT-TAP). Limited impact on bleeding time was observed for both agents. These results substantiate the independent contribution of both SCE5 and TAP toward inhibition of venous thrombus formation,

with maximum potency observed with administration of the SCE5-TAP fusion construct (Supplemental Figure 13 and Figure 6C).

## Discussion

The risk of recurrent coronary/cerebrovascular ischemia or VTE remains high, but strategies that utilize combined antiplatelet and anticoagulant therapy for these or other conditions carry a substantial risk of major bleeding with incomplete protection of thrombotic risk. In the current study, we report a strategy to target activated platelets and enrich antiplatelet and anticoagulant agents at the site of thrombus formation — but after initial platelet adhesion has been established. We have engineered a dual pathway inhibitor, SCE5-TAP, which consists of a single-chain antibody, SCE5, that targets and blocks the activated GPIIb/IIIa complex and TAP, a potent direct inhibitor of coagulation FXa. SCE5-TAP, administered through i.v. or s.c. routes, demonstrated selective platelet targeting and inhibition of thrombosis in murine models of both carotid artery and IVC thrombosis, without significant impact on hemostasis. Clinical effectiveness following s.c. administration represents a significant advantage. However further study is warranted to characterize parameters that may impact pharmacokinetics, such as volume limitations, retention at site of injection, and stability. With selective and site-specific targeting to activated platelets after platelet plug formation, we present a potentially novel strategy to broaden the therapeutic potential of dual pathway inhibition with improved safety.

We have previously demonstrated that the activated GPIIb/IIIa receptor presents suitable neoepitopes for targeting activated platelets, both diagnostically and therapeutically (34, 35). The GPIIb/IIIa complex is the most abundant protein expressed on the platelet surface. In addition, the conformational change of GPIIb/IIIa upon platelet activation from a low- to high-affinity fibrinogen binding state has allowed the identification of a single-chain antibody, SCE5, that selectively binds activated platelets but not to nonactivated platelets in circulation (21). Selective targeting to activated platelets ensures enrichment at a growing thrombus and reduces bleeding risk associated with current, clinically available inhibitors of GPIIb/IIIa, such as abciximab, Ept, and tirofiban, which are not conformation specific and exert an inhibitory effect on all platelets. Moreover, we have previously demonstrated by IVM, and corroborate within this report, the distinct delay between platelets forming an initial monolayer and the activation of GPIIb/IIIa (22). Mechanistically, this delay may be explained by recent reports describing shear-induced mechanosensitive platelet adhesion, which occurs without detectable activation markers, such as shape change, calcium signaling, and  $\alpha$ -granule secretion (18–20). Furthermore, SCE5 blockade of activated GPIIb/IIIa does not inhibit GPIIb- and GPVI-mediated platelet adhesion to exposed matrix proteins and VWF. Likewise, platelet adhesion to immobilized fibrinogen can be mediated through nonactivated GPIIb/IIIa. Therefore, activated GPIIb/IIIa presents an ideal epitope to target platelet thrombi with limited risk of impeding early events in matrix-driven adhesion or shear-induced adhesion that are critical to hemostasis.

To generate a dual pathway therapeutic, we combined the antiplatelet activity of SCE5 with the anticoagulant activity of TAP. TAP is a tight-binding serine protease inhibitor, specific for FXa, that was isolated from the soft tick *Ornithodoros moubata* (28). The relatively small size of TAP (60 amino acid residues) combined with strict specificity to FXa, which is a rate-limiting component in thrombin generation (36), makes it an ideal anticoagulant for recombinant fusion and expression. Indeed, we have previously demonstrated the feasibility of N-terminal TAP fusion and explored strategies for enrichment at sites of thrombus formation, including targeting to platelet ligand-induced binding sites (LIBS) (37, 38). Notably, the first-generation platelet-targeted TAP fusion construct, LIBS-TAP, was designed as a single pathway FXa inhibitor using the single-chain antibody, LIBS, that homes to activated platelets, but without inhibiting platelet activation or aggregation. Here, we extend the strategy of platelet targeting toward the development of a more potent dual pathway antithrombotic that combines and complements the anticoagulant activity of TAP with antiplatelet blockade through inhibition of activated GPIIb/IIIa. Indeed, enhanced thrombotic protection was observed with SCE5-TAP. Low dose SCE5-TAP (0.03  $\mu\text{g/g}$ ) administration displayed a 2-fold extension of carotid artery occlusion time (24.8 min vs. 12.5 min) as compared with identical administration of the single pathway inhibitor, LIBS-TAP, with similar levels of preserved hemostasis (37). Consistent with the clinical translation of a biotherapeutic using a xenogeneic peptide, immunogenicity presents a potential limitation to the application of TAP, and future studies examining immunogenicity are warranted. Additional limitations exist in generalizing the results of mouse models to predict bleeding risk in humans.

Inhibitors of coagulation FXa and FIIa offer a number of advantages over conventional vitamin K antagonists. However, the relative merit of FXa inhibition in contrast to direct thrombin inhibition remains an area of active debate (39, 40). The governing role of amplification in coagulation suggests greater antithrombotic potential with upstream inhibition of FXa. In addition, FXa inhibition may be associated with a reduced risk of undesirable pleiotropic effects. Thrombin is a key regulator of both hemostatic and nonhemostatic processes mediated through activation of protease-activated receptors (PARs). Targeting FXa inhibition to the platelet surface is a very attractive therapeutic strategy. Prothrombinase-driven activation of prothrombin to thrombin depends upon complexation of FXa and FVa on the acidic phosphatidylserine membrane surface of activated platelets. Likewise, the procoagulant activity of residual thrombin is dependent on de novo activation of prothrombin mediated by prothrombinase. As a unique fusion construct, SCE5-TAP combines potent anti-FXa activity with selective inhibition of activated platelets in a single molecule. This establishes an innovative dual pathway therapeutic with the clinically crucial advantage of preserved hemostasis.

A number of novel approaches have been explored to increase the effectiveness of antithrombotic therapy while reducing the risk of major bleeding. Bifunctional recombinant biologicals are particularly attractive for the prevention of thrombosis. RBCs have been modified either by direct chemical conjugation (41) or by antibody targeting (42, 43) to serve as carriers of plasminogen activators or thrombomodulin. While promising results have been reported, RBCs are not rapidly and selectively recruited to sites of incipient thrombus formation, and a requirement for repetitive parenteral administration of red cells seems impractical for sustained prophylaxis. Given the pivotal role of platelets in thrombus formation, a number of platelet-targeting schemes have been explored for drug and nanoparticle delivery to sites of thrombus formation, including peptide fragments that target GPIIb (44), GPIIb/IIIa (45), and P-selectin (46). All of these approaches have suffered from incomplete targeting and the need for relatively high circulating drug concentrations. For example, despite the report of single or multiple RGD motifs as targeting agents, clot prevention was modest and systemic bleeding times elevated (45). A fusion construct of urokinase to a single-chain antibody targeted to GPIIb was also recently described that bound to nonactivated circulating platelets (47). Collagen-targeted GPVI-CD39 represents an alternative strategy, targeting the antiplatelet ADPase CD39 to collagen fibers in the vessel wall. Notably, this promising approach relies on lesion enrichment of CD39 prior to platelet aggregation (48). Similarly, blockade of the intrinsic coagulation pathway has been investigated through the development of antibody, peptide, or antisense inhibitors of FXII (49, 50) and FXI (51, 52) as a means to reduce the risk of thrombosis without interfering with hemostasis. While promising results have been reported, conflicting studies suggest that FXII inhibition may be associated with an increased risk of thrombosis and embolization (53, 54) and FXI inhibition may be effective at only very low-surface concentrations of tissue factor. Finally, 2 recent reports explore multifunctional antithrombotics that demonstrate dual specificity, inhibiting platelet aggregation and FXa. Small molecule N-acetyldopamine dimer, isolated from grasshopper *Oxya chinensis sinuosa*, and 11-mer peptide ACH-11, isolated from *Aglkistrodon acutus* venom, were both described with inhibitory activity against FXa and platelet aggregation (55, 56). The dual inhibitory mechanism described in these reports differs significantly from SCE5-TAP, which is composed of an N-terminal scFv domain that inhibits activated GPIIb/IIIa, fused to a C-terminal TAP domain. Indeed, as a single fusion protein, SCE5-TAP can achieve independent inactivation of either target or simultaneous inhibition of both targets with unambiguous clot-specific enrichment.

Despite advances in antithrombotic therapy, recurrent thromboembolic events involving the arterial and venous circulation remain high. At the same time, current clinical strategies that combines antiplatelet and anticoagulant therapy to achieve increased antithrombotic efficacy carries a substantial risk of major bleeding with incomplete protection of thrombotic risk. Selective targeting to activated platelets provides a means to enrich antiplatelet and anticoagulant drug activity at the site of thrombus formation, but after the initial sealing platelet layer has been established and at low systemic concentrations that do not impair hemostasis. This approach represents a potentially novel and attractive strategy to break the link between high antithrombotic efficacy and bleeding complications.

## Methods

*Cloning, expression, and purification.* SCE5 was previously identified by phage display using depletion and selection protocols to isolate an scFv antibody that targets and blocks the activated GPIIb/IIIa complex — importantly, on both mouse and human platelets (21). A nonbinding control scFv, MUT, was generated through alanine substitution mutagenesis of the scFv heavy-chain complexity determining region

(CDR3) mutation (RND to AND), effectively eliminating GPIIb/IIIa binding (21). TAP was designed according to published sequence information (28) with inclusion of restriction sites BgIII and XbaI for ligation into pHOG21. To generate fusion constructs, TAP was cloned in frame to the C-terminus of SCE5 or MUT in pHOG21 to generate SCE5-TAP and MUT-TAP. Both SCE5 and MUT were subcloned from pHOG21 into a *Drosophila* expression vector pMT/BiP/V5-His (Invitrogen), using restriction sites NcoI and ApaI. Constructs were housed in *E. coli* BL21. All recombinant constructs were expressed in *Drosophila melanogaster* Schneider 2 (S2) cells using the expression vector pMT/BiP/V5-His with a copper-inducible metallothionein promoter for expression, a signal sequence for secretion, and a 6× His tag for purification. S2 cells were cultured in Express Five (Thermo Fisher Scientific) media to a density of  $1 \times 10^6$  cells/ml with a viability greater than 95%. Transfection was performed with 400 ng/ml of DNA and 100 µg/ml of dimethyldioctadecylammonium bromide (DDAB, MilliporeSigma). The DNA/DDAB mixture was incubated 20 minutes prior to addition to S2 culture. At day 4 after transfection, cells were supplemented with 500 µM copper sulfate to induce expression. Three days later, cells were centrifuged (8,000 g, 15 min, 4°C) and supernatant was collected for protein purification. Chelating sepharose chromatography (20 ml bed volume, 5 ml/min flow rate, GE Healthcare) was used to collect the copper sulfate with the attached recombinant fusion molecule from the supernatant (57). The column was washed to baseline with PBS, 0.5 M NaCl, and 10 mM imidazole in 50 mM Tris, pH 8.0, to remove nonspecifically bound proteins. Elution was carried out with 50 mM imidazole in 50 mM Tris, pH 8.0. Fractions were collected, and those containing significant amounts of product were pooled and dialyzed against PBS. Proteins were repurified using nickel-based affinity chromatography (BioLogic DuoFlow FPLC). As a final polishing step, size exclusion chromatography was performed using a HiPrep 16/60 Sephacryl S-200 HR column (GE Healthcare) with a flow rate of 1 ml/min with PBS as eluent. Purified constructs were characterized via SDS-PAGE with Coomassie blue total protein stain, and Western blot was performed with horseradish peroxidase-conjugated His tag monoclonal antibody (PentaHis, Qiagen). Final yield was approximately 3 mg/l.

**Platelet preparation.** Mouse blood was collected in citrate via cardiac puncture under the approval of the BIDMC Animal Care and Use Committee. Normal human blood draws were collected in citrate under approval of the BIDMC IRB. Platelet-rich plasma (PRP) was isolated by centrifugation at 300 g at room temperature for 10 minutes. Washed platelets were prepared by diluting PRP (1:20) in citrate wash buffer (11 mM glucose, 128 mM NaCl, 4.3 mM NaH<sub>2</sub>PO<sub>4</sub>, 7.5 mM Na<sub>2</sub>HPO<sub>4</sub>, 4.8 mM sodium citrate, 2.4 mM citric acid, 0.35% w/v BSA, pH 6.5). Samples were centrifuged at 1,200 g for 5 minutes and washed in citrate wash buffer. The washed platelets were resuspended in modified Tyrode's buffer (134 mM NaCl, 0.34 mM Na<sub>2</sub>HPO<sub>4</sub>, 2.9 mM KCl, 12 mM NaHCO<sub>3</sub>, 20 mM HEPES, 5 mM glucose, 0.35% w/v BSA, pH 7.0) to obtain a final concentration of 100,000 platelets/µl and 1 mM CaCl<sub>2</sub>.

**Platelet flow cytometry and aggregometry.** Flow cytometry was performed on the LSR II (BD Biosciences) or the FACS Calibur (BD Biosciences) with 50 µl PRP diluted 1:20 in modified Tyrode's buffer. scFv (10 µg/ml) targeting was characterized to resting platelets and to platelets activated with 20 µM ADP, 5 µg/ml CRP, or 30 µmol/l TRAP. Secondary staining was performed using 10 µl/ml Alexa-Fluor 488 (AF488) anti-His tag antibody (PentaHis, Qiagen) directed against the His tag of the scFv. In some assays, platelet activation was confirmed by PAC1-FITC (BD Biosciences, 340507) or CD62P-PE (BD Biosciences, 555524) staining. Fibrinogen binding to activated platelets in the presence or absence of an scFv was determined with a polyclonal FITC-labeled rabbit anti-fibrinogen antibody (Emfret, catalogue P140-1). Platelets were activated with 20 µM ADP in the presence of 3 µg/ml anti-fibrinogen antibody and SCE5, SCE5-TAP, or MUT-TAP added at a concentration of 15 µg/ml. Fibrinogen binding was recorded as mean fluorescence intensity (MFI), and data were reported as percent inhibition relative to maximum binding observed to 20 µM ADP-activated platelets in buffer control samples. Where indicated, fibrinogen binding was also characterized using AF488-labeled fibrinogen (Molecular Probes F13191), as previously reported (58). Data were analyzed using FlowJo software, and all experiments were performed in triplicate.

Light transmission aggregometry was performed as previously reported (58) with 100 µl PRP; incubated with SCE5, SCE5-TAP, or MUT-TAP; and then activated with 10 µM ADP. Platelet-poor plasma (PPP) was obtained after centrifugation of PRP (1,000 g, 10 min). Samples were measured for 10 minutes.

**FXa activity assay.** Purified TAP fusion constructs were characterized for their ability to inhibit FXa in solution using chromogenic substrate Spectrozyme FXa (Sekisui Diagnostics). Briefly, 165 µl of recombinant construct (100 nM) was incubated with 10 µl of 500 pM FXa and 10 µl of 5 mM Spectrozyme FXa in 50 mM Tris buffer, at pH 8.4 and 37°C for 10 minutes. Reactions were stopped with the addition of 20%

acetic acid to a final concentration of 5%, and absorbance was measured at 405 nm. Absorbance values generated in vehicle control were considered to have maximum FXa activity, and results are presented as percent inhibition of this activity. Anti-FXa activity was also assessed after targeting constructs to fibrinogen-adherent platelets. Microwell plates were coated overnight with 100 µg/ml of purified fibrinogen (MilliporeSigma), blocked with 1% BSA, and gently washed 3 times with modified Tyrode's buffer. Citrate-washed platelets were resuspended in modified Tyrode's buffer containing 1 mM CaCl<sub>2</sub> and incubated for 30 minutes on fibrinogen-coated wells. SCE5, SCE5-TAP, or MUT-TAP (0.2 mg/ml) were added to fibrinogen-adherent platelets and incubated for 30 minutes. Following incubation, supernatant was removed and surfaces were gently washed with modified Tyrode's buffer. FXa activity was measured using SpectrozymeFXa, as described above. Absorbance values generated with vehicle control were considered to have maximum FXa activity, and results are presented as percent inhibition of this activity. Circulating anti-FXa activity, including peak circulating anti-FXa activity, was measured in mouse plasma using the Actichrome Heparin Anti-FXa kit (Sekisui Diagnostics). A standard curve was generated with the LMWH Lovenox (enoxaparin sodium injection, Sanofi) with defined anti-FXa units of activity. Results were reported as anti-FXa units (U) of activity/ml.

*Platelet adhesion to collagen under flow.* Flow-chamber adhesion assays were performed in a rectangular glass capillary (10 mm length × 2 mm width × 0.2 mm height) flow chamber (Vitrotubes). The glass capillaries were coated with collagen fibers by overnight incubation in a collagen (100 µg/ml) solution (Takeda), followed by a blocking step in 1% BSA. Whole blood was collected in sodium citrate and recalcified. A total of 5 or 15 µg/ml of SCE5, SCE5-TAP, MUT-TAP, or PBS control was added to calcified whole blood, followed by perfusion through collagen-coated glass capillaries to form microthrombi at a shear-rate of 500 s<sup>-1</sup> (5 dyn/cm<sup>2</sup>) for 5 minutes (PHD 2000, Harvard Apparatus). PBS was then perfused through the glass capillaries for 10 minutes to remove unbound cells, and microthrombi were visualized with bright field microscopy (20× objective) using the IX81 Olympus microscope (Olympus) and Cell<sup>^</sup>P 1692 software. Images were analyzed with ImageJ, and results are reported as percent area covered by platelets.

*FeCl<sub>3</sub>-induced carotid artery occlusion.* C57BL/6 mice (Charles River Laboratories; 22–25 grams) were anesthetized with i.p. administration of ketamine (100 mg/kg) and xylazine (5 mg/kg) and placed under a dissecting microscope. The left common carotid artery was dissected from connective tissue. Experimental reagents were administered i.v. (100 µl, jugular) 5 minutes prior to initiation of thrombosis, including saline vehicle control, SCE5 (0.3 µg/g), MUT-TAP (0.03 and 0.3 µg/g), SCE5-TAP (0.03 and 0.3 µg/g), LMWH (10 µg/g), and Ept (10 µg/g). To induce thrombosis, filter paper (1 × 2 mm), saturated with 10% FeCl<sub>3</sub>, was placed under the left common carotid artery for 3 minutes. Following a 3-minute exposure period, the area was flushed with saline and a nano Doppler-flow probe (0.5 VB, Transonic) was positioned to record flow (T106, Transonic). Flow speed was recorded for up to 30 minutes, and occlusion was defined as a decrease in flow to 0.0 ± 0.2 ml/min. To assess bleeding risk, agents were administered (100 µl, i.v. jugular) 1 minute prior to tail transection for determination of bleeding time and bleeding volume measurements. A detailed protocol for tail transection and bleeding risk assessment is described below.

*In vivo imaging.* SCE5-TAP and MUT-TAP were labeled with NHS-IR800 dye (1:5 molar ratio, Pierce) for 1 hour at room temperature, according to manufacturer's instructions, and purified over a desalting column. Agent administration and initiation of carotid artery thrombosis were performed as described above. Animals were imaged 2 hours after the administration of the labeled agent (1 µg/g, i.v.) using an IVIS Lumina Series II Imaging System (Caliper Life Sciences). Fluorescent images were obtained by a charge-coupled device (CCD) camera using the XFO-12 fluorescence equipment (excitation filter, 710–760 nm; emission filter, 810–875 nm) on automated exposure time. Photographic pictures were also obtained during illumination. Overlays of fluorescence and photographic images, as well as processing and analysis, were performed using Living Image 4.4 software.

*EIM.* The EIM was used to determine the effectiveness of test agents to prevent nonocclusive venous thrombosis, as previously described (33, 59). Saline, SCE5-TAP (0.5–1.5 µg/g s.c.), LMWH (2–6 µg/g s.c.), or rivaroxaban (0.5–1.5 µg/g per os) were administered 4 hours prior to electrolytic injury and 24 hours after injury. C57BL/6 mice, weighing 22–25 grams, were anesthetized with 2% isoflurane, and the IVC was exposed via a midline laparotomy. Venous side branches were either ligated using 7-0 Prolene suture (Ethicon Inc.) or cauterized using Change-a-tip (Bovie medical), while posterior branches were left patent. A 25-gauge stainless-steel needle, attached to a silver-coated copper wire (KY-30-1-GRN, Electrospec) was inserted into the exposed caudal IVC and positioned against the anterior wall (anode).

A second wire was implanted s.c. to complete the circuit (cathode). A current of 250  $\mu$ Amps over 15 minutes was applied using a Grass S48 square wave stimulator and a constant current unit (Grass Technologies, Astro-Med Inc.). In sham animals, the needle was placed into the IVC for 15 minutes without application of current. After 15 minutes, the needle was removed and a cotton swab was placed in contact with the puncture site to prevent bleeding. The laparotomy was closed with 5-0 vicryl suture (Ethicon Inc.) and skin approximated using a tissue adhesive glue (Vetbond, 3M). Forty-eight hours after injury, the IVC was excised from below the renal veins to just above the bifurcation to determine the wet TW, as well as to characterize the thrombus using flow cytometry and histology. The IVC was imaged using a stereoscope Zeiss Axio Zoom V16 with 8 $\times$  magnification.

*Ex vivo thrombus flow cytometry.* The IVC and thrombus were finely minced and shaken for 60 minutes at 37°C in 1 ml of RPMI-1640 supplemented with 10% FBS, 62.5 U/ml collagenase VII (MilliporeSigma), and 0.625 U/ml Dispase (BD Biosciences). Isolated cells were passed through a 70- $\mu$ m cell strainer to remove debris. Collected cells were separated by centrifugation (300 g for 10 min) at room temperature. The supernatant was removed and erythrocytes were lysed in 9 ml of DI-water for 7 seconds, followed by 1 ml of 10 $\times$  PBS. Cells were counted and stained according to standard protocol. Antibodies included APC rat anti-mouse CD45 (clone 30-F11, BD Biosciences), Pacific Blue rat anti-mouse CD11b (clone M1/70.15, eBioscience), PE rat anti-mouse Ly6G (clone 1A8, BD Biosciences), and PE rat anti-mouse CD41 (clone MWReg30, BD Biosciences). Isotype IgG was included as a negative control for each marker. Cell suspensions were analyzed using a BD LSRII 4-laser benchtop analyzer.

*Bleeding time and blood loss measurement.* Animals were anesthetized with i.p. administration of ketamine HCl (Zoetis, 125 mg/kg) and xylazine (Akorn Inc., 12.5 mg/kg). Bleeding time and volume were assessed by transection of the tail, 10 mm from its end, using a blade (60). The tail was immediately immersed in a 50 ml Falcon tube containing warm saline (37°C). The tail was positioned vertically with the tip 2 cm below the body horizon. The time at which the tail first stopped bleeding for 30 seconds was recorded as bleeding time. Blood loss was determined by measuring hemoglobin concentration after erythrocyte lysis. Collected blood cells were separated by centrifugation (300 g for 10 min at room temperature). The supernatant was removed and erythrocytes lysed in 9 ml of DI-water for 7 seconds followed by the addition of 1 ml of 10 $\times$  PBS. The concentration of hemoglobin was determined spectrophotometrically by measuring absorbance at 550 nm. Blood volume was calculated using a hemoglobin standard curve. Measurements were performed to correlate with agent administration in the FeCl<sub>3</sub>-induced carotid artery occlusion model 1 minute after i.v. administration and, in the EIM, 4 hours after s.c. or per os administration, as indicated.

*IHC.* Specimens were fixed overnight in 10% neutral buffered formalin, processed for paraffin embedding, and 5  $\mu$ m sections were stained with H&E. Additional staining was performed for platelets (rabbit anti-mouse CD41, clone MWReg30, Abcam), neutrophils (Naphthol AS-D Chloroacetate Esterase, MilliporeSigma), and monocytes (rabbit anti-mouse CD68, Abcam, catalogue ab125212). Images were taken from 3–5 representative sections from each group ( $n = 4$ ) using Olympus BX41 at 10 $\times$  and 40 $\times$  magnification. To characterize thrombus area, the IVC ( $n = 5$ ) was sectioned 48 hours after injury, stained with H&E, and examined under light microscopy (Olympus BX41). The area of the venous thrombus was analyzed using Image J 1.46r (NIH) from H&E-stained specimens (3 sections/mouse) at the point of greatest luminal stenosis. To eliminate variability between groups, thrombus area was normalized to aortic wall thickness and reported as thrombus area (mm<sup>2</sup>)/aorta wall thickness (mm) (33).

*IVM.* Surgical preparation of the mouse cremaster muscle microcirculation for IVM was performed as previously described (61, 62). Briefly, C57BL/6 mice were anesthetized with i.p. administration of ketamine HCl (125 mg/kg), xylazine (12.5 mg/kg), and atropine (0.25 mg/ml) and placed on a 37°C surgical blanket. The jugular vein was cannulated with PE 10 tubing to allow introduction of reagents, including anti-CD42b-Dylight 649 (Emfret Analytics, catalog M040-3), SCE5-TAP, MUT-TAP, LMWH, or saline vehicle control. In selected studies, therapeutics were delivered s.c. 4 hours or 24 hours prior to cremaster exteriorization and laser injury, as indicated. For colocalization studies, SCE5-TAP and MUT-TAP were preincubated (10  $\mu$ g/ml, 10 min) with penta-His AF488 Conjugate (Qiagen, catalogue 35310). The cremaster muscle was exteriorized, pinned to the stage, and superfused with therma-controlled bicarbonate buffered saline equilibrated with 5% CO<sub>2</sub> in N<sub>2</sub>. Between 5 and 30 minutes after infusion of the platelet label (anti-CD42b-Dylight 649), injury to a cremaster arteriolar or venular vessel wall was induced with a Micropoint Laser System (Photonic Instruments) focused through the microscope objective parfocal with the focal point and tuned to 440 nm. Microvessel data were obtained using an Olympus AX microscope

with a 60× water immersion objective recorded with a Hamamatsu C11440 Digital Camera. Image acquisition and data analysis were performed using SlideBook software (Intelligent Imaging Innovations). For each treatment group, platelet accumulation was characterized as median integrated fluorescence plotted over 3 minutes from thrombi ( $n = 25\text{--}35$ ) generated in 4–5 mice. In addition, platelet signals were quantified as AUC for each individual thrombus plotted against time (63).

**Statistics.** Data are presented as mean  $\pm$  SD for the indicated experimental groups. Statistical comparisons were performed with 1-way ANOVA, and post hoc testing was performed using Bonferroni's modification of 2-tailed Student's *t* test for multiple comparisons or 2-tailed *t* test for paired comparisons using GraphPad Prism 5.0 (GraphPad Software Inc.). Significance was indicated as  $*P \leq 0.05$ ,  $**P \leq 0.01$ , and  $***P \leq 0.001$ .

**Study approval.** Human blood samples were obtained from healthy volunteers, who provided written informed consent. Studies were approved by the BIDMC IRB. All animal experiments were approved by the Animal Care and Use Committee of BIDMC and The Alfred Medical Research and Education Precinct – Baker Heart and Diabetes Institute. All investigators adhered to NIH guidelines for the care and use of laboratory animals. All experiments were performed in the BIDMC Center for Hemostasis and Thrombosis Research Core.

### Author contributions

DHP, CH, and XW contributed equally to this work. KP and ELC jointly served as senior authors in direction of this project. XW, PJ, TB, and CEH were responsible for scFv construction and expression/purification. XW, BL, JY, AS, and KP were responsible for in vitro validation and in vivo validation in arterial models. DHP, CH, ED, LL, and ELC were responsible for in vitro validation, IVM data, and in vivo validation in venous models. CH, DHP, XW, CEH, KP, and ELC wrote the manuscript.

### Acknowledgments

We thank Glenn Merrill-Skoloff (BIDMC Center for Hemostasis and Thrombosis Research Core) for assistance with IVM. We thank Shirley K. Wroblewski and Jose A. Diaz (Conrad Jobst Vascular Research Laboratories, University of Michigan) for training assistance in the EIM of venous thrombosis. We acknowledge support from the NIH (R01HL128237) for ELC, the Juvenile Diabetes Research Foundation with Postdoctoral Fellowship (3-PDF2014-188-A-N) for DHP, the William Harvey Research Institute-Academy with Fellowship for TB, the National Heart Foundation of Australia for XW and CEH, and the National Health and Medical Research Council of Australia for KP.

Address correspondence to: Elliot L. Chaikof, 110 Francis Street, Suite 9F, Boston, Massachusetts 02215, USA. Phone: 617.632.9581; Email: echaikof@bidmc.harvard.edu.

DHP's present address is: Department of Aerospace and Mechanical Engineering and Department of Chemical and Biomolecular Engineering, University of Notre Dame, Notre Dame, Indiana, USA.

PJ's present address is: Klinikum Westmuensterland, 46325 Borken, Germany.

TB and CEH's present address is: Australian Centre for Blood Diseases, Monash University, Melbourne, VIC, Australia.

- 
1. Mehta SR, et al. Effects of pretreatment with clopidogrel and aspirin followed by long-term therapy in patients undergoing percutaneous coronary intervention: the PCI-CURE study. *Lancet*. 2001;358(9281):527–533.
  2. Wallentin L, et al. Ticagrelor versus clopidogrel in patients with acute coronary syndromes. *N Engl J Med*. 2009;361(11):1045–1057.
  3. Connolly SJ, et al. Dabigatran versus warfarin in patients with atrial fibrillation. *N Engl J Med*. 2009;361(12):1139–1151.
  4. Granger CB, et al. Apixaban versus warfarin in patients with atrial fibrillation. *N Engl J Med*. 2011;365(11):981–992.
  5. Patel MR, et al. Rivaroxaban versus warfarin in nonvalvular atrial fibrillation. *N Engl J Med*. 2011;365(10):883–891.
  6. Alexander JH, et al. Apixaban with antiplatelet therapy after acute coronary syndrome. *N Engl J Med*. 2011;365(8):699–708.
  7. Dans AL, et al. Concomitant use of antiplatelet therapy with dabigatran or warfarin in the Randomized Evaluation of Long-Term Anticoagulation Therapy (RE-LY) trial. *Circulation*. 2013;127(5):634–640.
  8. Lamberts M, et al. Oral anticoagulation and antiplatelets in atrial fibrillation patients after myocardial infarction and coronary

- intervention. *J Am Coll Cardiol*. 2013;62(11):981–989.
9. Sørensen R, et al. Risk of bleeding in patients with acute myocardial infarction treated with different combinations of aspirin, clopidogrel, and vitamin K antagonists in Denmark: a retrospective analysis of nationwide registry data. *Lancet*. 2009;374(9706):1967–1974.
  10. Steinberg BA, et al. Use and associated risks of concomitant aspirin therapy with oral anticoagulation in patients with atrial fibrillation: insights from the Outcomes Registry for Better Informed Treatment of Atrial Fibrillation (ORBIT-AF) Registry. *Circulation*. 2013;128(7):721–728.
  11. Xu H, et al. Concomitant Use of Single Antiplatelet Therapy With Edoxaban or Warfarin in Patients With Atrial Fibrillation: Analysis From the ENGAGE AF-TIMI48 Trial. *J Am Heart Assoc*. 2016;5(2).
  12. Franchi F, Angiolillo DJ. Novel antiplatelet agents in acute coronary syndrome. *Nat Rev Cardiol*. 2015;12(1):30–47.
  13. Alexander JH, et al. Apixaban vs. warfarin with concomitant aspirin in patients with atrial fibrillation: insights from the ARIS-TOTLE trial. *Eur Heart J*. 2014;35(4):224–232.
  14. Goodman SG, et al. Factors associated with major bleeding events: insights from the ROCKET AF trial (rivaroxaban once-daily oral direct factor Xa inhibition compared with vitamin K antagonism for prevention of stroke and embolism trial in atrial fibrillation). *J Am Coll Cardiol*. 2014;63(9):891–900.
  15. Hernandez I, Baik SH, Piñera A, Zhang Y. Risk of bleeding with dabigatran in atrial fibrillation. *JAMA Intern Med*. 2015;175(1):18–24.
  16. Sherwood MW, et al. Use of Dual Antiplatelet Therapy and Patient Outcomes in Those Undergoing Percutaneous Coronary Intervention: The ROCKET AF Trial. *JACC Cardiovasc Interv*. 2016;9(16):1694–1702.
  17. Capodanno D, Angiolillo DJ. Management of antiplatelet and anticoagulant therapy in patients with atrial fibrillation in the setting of acute coronary syndromes or percutaneous coronary interventions. *Circ Cardiovasc Interv*. 2014;7(1):113–124.
  18. Nesbitt WS, et al. A shear gradient-dependent platelet aggregation mechanism drives thrombus formation. *Nat Med*. 2009;15(6):665–673.
  19. Ruggeri ZM, Orje JN, Habermann R, Federici AB, Reininger AJ. Activation-independent platelet adhesion and aggregation under elevated shear stress. *Blood*. 2006;108(6):1903–1910.
  20. Bellido-Martín L, Chen V, Jasuja R, Furie B, Furie BC. Imaging fibrin formation and platelet and endothelial cell activation in vivo. *Thromb Haemost*. 2011;105(5):776–782.
  21. Schwarz M, et al. Conformation-specific blockade of the integrin GPIIb/IIIa: a novel antiplatelet strategy that selectively targets activated platelets. *Circ Res*. 2006;99(1):25–33.
  22. Hohmann JD, et al. Delayed targeting of CD39 to activated platelet GPIIb/IIIa via a single-chain antibody: breaking the link between antithrombotic potency and bleeding? *Blood*. 2013;121(16):3067–3075.
  23. Dewilde WJ, et al. Use of clopidogrel with or without aspirin in patients taking oral anticoagulant therapy and undergoing percutaneous coronary intervention: an open-label, randomised, controlled trial. *Lancet*. 2013;381(9872):1107–1115.
  24. Mega JL, et al. Rivaroxaban in patients with a recent acute coronary syndrome. *N Engl J Med*. 2012;366(1):9–19.
  25. Perzborn E, Heitmeier S, Laux V. Effects of Rivaroxaban on Platelet Activation and Platelet-Coagulation Pathway Interaction: In Vitro and In Vivo Studies. *J Cardiovasc Pharmacol Ther*. 2015;20(6):554–562.
  26. Tricoci P, et al. Thrombin-receptor antagonist vorapaxar in acute coronary syndromes. *N Engl J Med*. 2012;366(1):20–33.
  27. McFadyen JD, Schaff M, Peter K. Current and future antiplatelet therapies: emphasis on preserving haemostasis. *Nat Rev Cardiol*. 2018;15(3):181–191.
  28. Waxman L, Smith DE, Arcuri KE, Vlasuk GP. Tick anticoagulant peptide (TAP) is a novel inhibitor of blood coagulation factor Xa. *Science*. 1990;248(4955):593–596.
  29. Wang X, Xu L. An optimized murine model of ferric chloride-induced arterial thrombosis for thrombosis research. *Thromb Res*. 2005;115(1-2):95–100.
  30. McRae SJ, Ginsberg JS. Initial treatment of venous thromboembolism. *Circulation*. 2004;110(9 Suppl 1):I3–I9.
  31. Schönfelder T, Jäckel S, Wenzel P. Mouse models of deep vein thrombosis. *Gefasschirurgie*. 2017;22(Suppl 1):28–33.
  32. Diaz JA, et al. Critical review of mouse models of venous thrombosis. *Arterioscler Thromb Vasc Biol*. 2012;32(3):556–562.
  33. Diaz JA, et al. The electrolytic inferior vena cava model (EIM) to study thrombogenesis and thrombus resolution with continuous blood flow in the mouse. *Thromb Haemost*. 2013;109(6):1158–1169.
  34. Kim W, et al. Targeted antithrombotic protein micelles. *Angew Chem Int Ed Engl*. 2015;54(5):1461–1465.
  35. Wang X, et al. Novel single-chain antibody-targeted microbubbles for molecular ultrasound imaging of thrombosis: validation of a unique noninvasive method for rapid and sensitive detection of thrombi and monitoring of success or failure of thrombolysis in mice. *Circulation*. 2012;125(25):3117–3126.
  36. Rand MD, Lock JB, van't Veer C, Gaffney DP, Mann KG. Blood clotting in minimally altered whole blood. *Blood*. 1996;88(9):3432–3445.
  37. Stoll P, et al. Targeting ligand-induced binding sites on GPIIb/IIIa via single-chain antibody allows effective anticoagulation without bleeding time prolongation. *Arterioscler Thromb Vasc Biol*. 2007;27(5):1206–1212.
  38. Hagemeyer CE, et al. Fibrin-targeted direct factor Xa inhibition: construction and characterization of a recombinant factor Xa inhibitor composed of an anti-fibrin single-chain antibody and tick anticoagulant peptide. *Thromb Haemost*. 2004;92(1):47–53.
  39. Ansell J. Factor Xa or thrombin: is factor Xa a better target? *J Thromb Haemost*. 2007;5 Suppl 1:60–64.
  40. Weitz JI. Factor Xa or thrombin: is thrombin a better target? *J Thromb Haemost*. 2007;5 Suppl 1:65–67.
  41. Murciano JC, Medinilla S, Eslin D, Atochina E, Cines DB, Muzykantov VR. Prophylactic fibrinolysis through selective dissolution of nascent clots by tPA-carrying erythrocytes. *Nat Biotechnol*. 2003;21(8):891–896.
  42. Zaitsev S, et al. Targeting recombinant thrombomodulin fusion protein to red blood cells provides multifaceted thromboprophylaxis. *Blood*. 2012;119(20):4779–4785.
  43. Zaitsev S, et al. Sustained thromboprophylaxis mediated by an RBC-targeted pro-urokinase zymogen activated at the site of clot formation. *Blood*. 2010;115(25):5241–5248.
  44. Doshi N, Orje JN, Molins B, Smith JW, Mitragotri S, Ruggeri ZM. Platelet mimetic particles for targeting thrombi in flowing blood. *Adv Mater Weinheim*. 2012;24(28):3864–3869.

45. Zhu Y, et al. Engineering Factor Xa Inhibitor with Multiple Platelet-Binding Sites Facilitates its Platelet Targeting. *Sci Rep.* 2016;6:29895.
46. Modery CL, Ravikumar M, Wong TL, Dzuricky MJ, Durongkaveroj N, Sen Gupta A. Heteromultivalent liposomal nanoconstructs for enhanced targeting and shear-stable binding to active platelets for site-selective vascular drug delivery. *Biomaterials.* 2011;32(35):9504–9514.
47. Fuentes RE, et al. A chimeric platelet-targeted urokinase prodrug selectively blocks new thrombus formation. *J Clin Invest.* 2016;126(2):483–494.
48. Degen H, et al. ADPase CD39 Fused to Glycoprotein VI-Fc Boosts Local Antithrombotic Effects at Vascular Lesions. *J Am Heart Assoc.* 2017;6(8).
49. Baeriswyl V, Calzavarini S, Gerschheimer C, Diderich P, Angelillo-Scherrer A, Heinis C. Development of a selective peptide macrocycle inhibitor of coagulation factor XII toward the generation of a safe antithrombotic therapy. *J Med Chem.* 2013;56(9):3742–3746.
50. Larsson M, et al. A factor XIIIa inhibitory antibody provides thromboprotection in extracorporeal circulation without increasing bleeding risk. *Sci Transl Med.* 2014;6(222):222ra17.
51. Büller HR, et al. Factor XI antisense oligonucleotide for prevention of venous thrombosis. *N Engl J Med.* 2015;372(3):232–240.
52. Tucker EI, et al. Prevention of vascular graft occlusion and thrombus-associated thrombin generation by inhibition of factor XI. *Blood.* 2009;113(4):936–944.
53. Renne T, et al. Defective thrombus formation in mice lacking coagulation factor XII. *J Exp Med.* 2005;202(2):271–281.
54. Mangal AK, Naiman SC. Hageman factor deficiency and oral contraceptives. *Lancet.* 1980;1(8171):774.
55. Chen M, et al. A Novel Direct Factor Xa Inhibitory Peptide with Anti-Platelet Aggregation Activity from *Agkistrodon acutus* Venom Hydrolysates. *Sci Rep.* 2015;5:10846.
56. Lee W, et al. Evaluation of novel factor Xa inhibitors from *Oxya chinensis sinuosa* with anti-platelet aggregation activity. *Sci Rep.* 2017;7(1):7934.
57. Lehr RV, Elefante LC, Kikly KK, O'Brien SP, Kirkpatrick RB. A modified metal-ion affinity chromatography procedure for the purification of histidine-tagged recombinant proteins expressed in *Drosophila* S2 cells. *Protein Expr Purif.* 2000;19(3):362–368.
58. Wang X, et al. Towards effective and safe thrombolysis and thromboprophylaxis: preclinical testing of a novel antibody-targeted recombinant plasminogen activator directed against activated platelets. *Circ Res.* 2014;114(7):1083–1093.
59. Diaz JA, et al. Electrolytic inferior vena cava model (EIM) of venous thrombosis. *J Vis Exp.* 2011;(53):e2737.
60. Liu Y, Jennings NL, Dart AM, Du XJ. Standardizing a simpler, more sensitive and accurate tail bleeding assay in mice. *World J Exp Med.* 2012;2(2):30–36.
61. Ley K, et al. Sequential contribution of L- and P-selectin to leukocyte rolling in vivo. *J Exp Med.* 1995;181(2):669–675.
62. Yang J, et al. Targeted gene disruption demonstrates that P-selectin glycoprotein ligand 1 (PSGL-1) is required for P-selectin-mediated but not E-selectin-mediated neutrophil rolling and migration. *J Exp Med.* 1999;190(12):1769–1782.
63. Falati S, Gross P, Merrill-Skoloff G, Furie BC, Furie B. Real-time in vivo imaging of platelets, tissue factor and fibrin during arterial thrombus formation in the mouse. *Nat Med.* 2002;8(10):1175–1181.